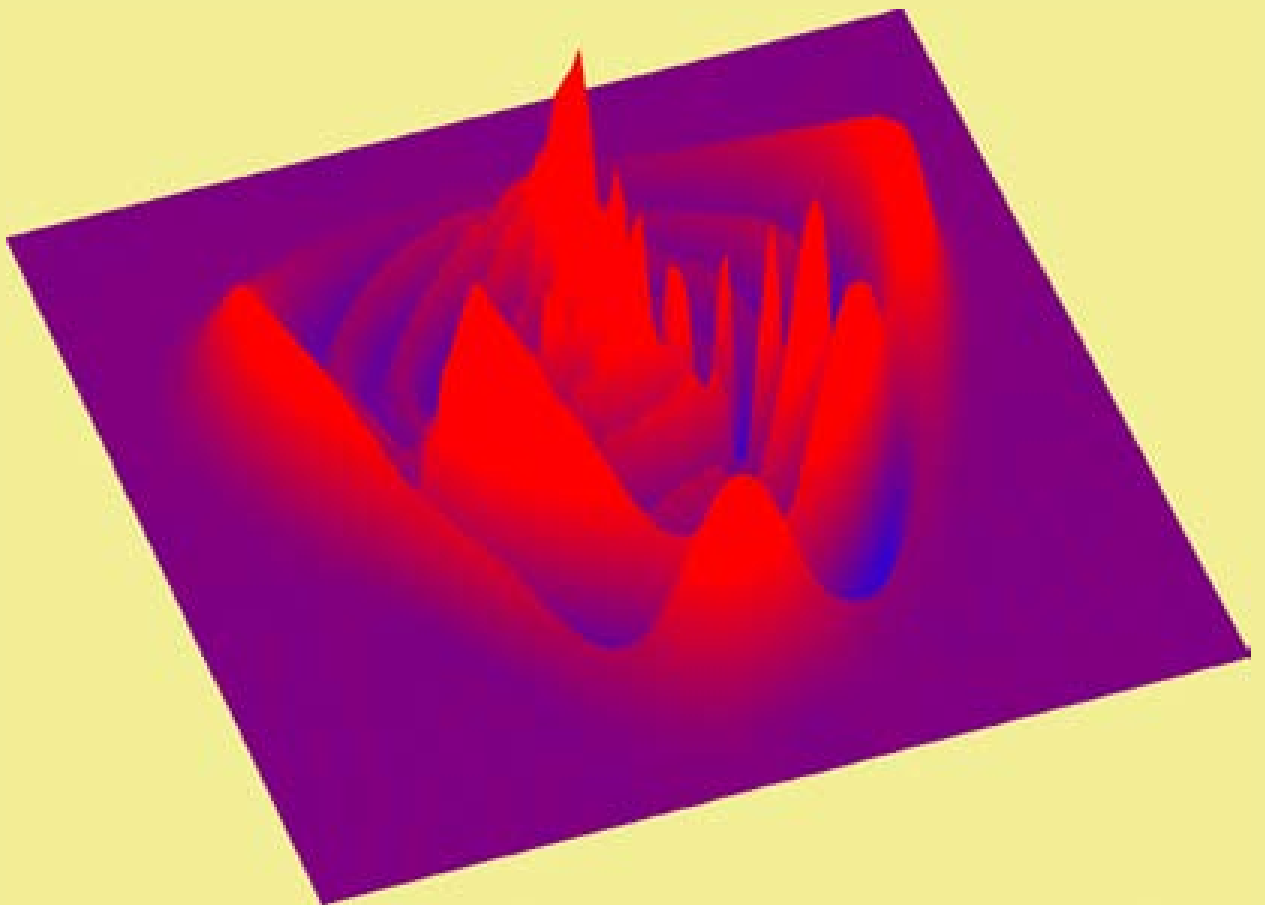


Coherent dynamics of small molecules in rare gas crystals

Markus Gühr



Cuvillier Verlag Göttingen

Coherent dynamics of small molecules
in rare gas crystals

im
Fachbereich Physik
der
Freien Universität Berlin
eingereichte Dissertation

vorgelegt von

Markus Gühr

Januar 2005

Bibliografische Information Der Deutschen Bibliothek

Die Deutsche Bibliothek verzeichnet diese Publikation in der Deutschen Nationalbibliografie; detaillierte bibliografische Daten sind im Internet über <http://dnb.ddb.de> abrufbar.

1. Aufl. - Göttingen : Cuvillier, 2005

Zugl.: Berlin, Univ., Diss., 2005

ISBN 3-86537-411-5

Diese Arbeit wurde in der Zeit von Oktober 2001 bis Dezember 2004 unter der Aufsicht von Herrn Prof. Dr. N. Schwentner am Fachbereich Physik der Freien Universität Berlin durchgeführt.

Erstgutachter: Prof. Dr. N. Schwentner

Zweitgutachter: Prof. Dr. L. Wöste

Drittgutachter: Prof. Dr. T. Elsässer

Disputationstermin: 16. Februar 2005

Picture on title: Wigner function of a $1/6$ revival (see Sec. 2.2.3)

© CUVILLIER VERLAG, Göttingen 2005

Nonnenstieg 8, 37075 Göttingen

Telefon: 0551-54724-0

Telefax: 0551-54724-21

www.cuvillier.de

Alle Rechte vorbehalten. Ohne ausdrückliche Genehmigung des Verlages ist es nicht gestattet, das Buch oder Teile daraus auf fotomechanischem Weg (Fotokopie, Mikrokopie) zu vervielfältigen.

1. Auflage, 2005

Gedruckt auf säurefreiem Papier

ISBN 3-86537-411-5

Kurzfassung

Die ultraschnelle Dynamik von Br_2 Molekülen in Argonkristallen ($\text{Br}_2:\text{Ar}$) wird mit Hilfe der Femtosekunden Anrege-Abfrage Methode zum ersten Male untersucht. In den zeitaufgelösten Spektren werden die kohärente intramolekulare Dynamik und eine kohärente Umgebungsdynamik beobachtet. Mit dem RKR Algorithmus wird die elektronische B Zustands-Potentialfläche des Br_2 konstruiert. Weiterhin wird die Energierelaxation in diesem Zustand quantifiziert. Während der ersten Kollision des Moleküls mit dem Käfig aus Edelgasatomen verliert das molekulare Schwingungswellenpaket bis zu 50 % seiner Energie. Die intramolekulare Kohärenz bleibt dennoch danach erhalten. Ebenso kann diese Kohärenz auch einen nicht-adiabatischen elektronischen Übergang überleben, was am Beispiel von I_2 in Kryptonkristallen ($\text{I}_2:\text{Kr}$) verdeutlicht wird.

Die feste Argon-Umgebung erzeugt Dekohärenz im Molekül, dennoch können Interferenzphänomene von molekularen Schwingungswellenpaketen kontrolliert werden. Mit Hilfe eines Computerprogramms zur Wellenpaket-Propagation wird ein neues Kontrollschema, basierend auf "gechirpten" Laserpulsen, erarbeitet ("chirp" = Änderung der Lichtfrequenz mit der Zeit). Die Erzeugung des Wellenpaketes mit negativ oder positiv linear "gechirpten" Laserpulsen erlaubt eine vor- bzw. rückwärtige Zeitverschiebung der normalen Wellenpaket-Propagation.

Darauf basiert ein hier erstmals vorgestelltes Schema zur Quantifizierung des molekularen Kohärenzzerfalls (Dephasierung). Die Wellenpakete werden unter Anregung mit negativ "gechirpten" Laserpulsen zu einem Zeitpunkt T_{opt} räumlich fokussiert. Aus dem Modulationskontrast bestimmen wir die Vibrations-Dephasierungszeit $T_{\text{deph}}^{\text{vib}} = 3$ ps im B Zustand. Diese entspricht etwa elf Schwingungsperioden von 280 fs. Die positiv "gechirpten" Pulse ziehen die molekularen Interferenzstrukturen ("revivals") bezüglich $T_{\text{deph}}^{\text{vib}}$ vor. Durch die kohärente Präparation von vier Schwingungszuständen mit einem positiv "gechirpten" Puls gelingt uns die Beobachtung eines 1/6 "revivals". Aus den Daten schließen wir auf eine Dephasierung der vier Niveaus in $T_{\text{vib}}^4 \approx 1.2$ ps. Der "chirp" verlängert den Laserpuls um einen Faktor zehn auf $\Delta\tau = 300$ fs. Die elektronische Dephasierungszeit $T_{\text{deph}}^{\text{el}}$ des optischen $\text{B} \leftarrow \text{X}$ Überganges engt die Kontrollmöglichkeit auf das Zeitintervall $\Delta\tau < T_{\text{deph}}^{\text{el}}$ ein. Die erfolgreiche Kontrolle erlaubt daher eine Abschätzung mit $T_{\text{deph}}^{\text{el}} > 300$ fs aus dem Experiment.

Eine langanhaltende, monochromatische Frequenz $f_{\text{P}} = 2$ THz wird in den molekularen Anrege-Abfrage Spektren des $\text{Br}_2:\text{Ar}$ beobachtet. Diese entspricht der Frequenz des Zonenrand-Phonons (ZBP) im Argonkristall. Weiterhin wird eine Frequenzkomponente von $f_{\text{P}} = 1.5$ THz im Fall von $\text{I}_2:\text{Kr}$ beobachtet, welche wiederum zum ZBP des Kryptonkristalls gehört. Weder der Absolutwert von f_{P} noch seine Phase hängt von der molekularen Schwingungsdynamik ab. Die Phononen werden nach dem DECP ("Displacive Excitation of Coherent Phonons") Schema beim elektronischen $\text{B} \leftarrow \text{X}$ und $\text{A} \leftarrow \text{X}$ Übergang angeregt. Eine Modellrechnung zeigt die Expansion der Elektronenhülle beim Übergang vom elektronischen Grundzustand X in den B oder A Zustand, wodurch die Edelgasatome in der Umgebung angestoßen werden. Eine Gruppe von Edelgasatomen in der (100) Ebene ist von der molekularen Schwingung entkoppelt. Die Zonenrand-Phononen haben eine verschwindend kleine Gruppengeschwindigkeit v_{g} . Daher bleibt ihre Amplitude in der Nähe des Moleküls lokalisiert, während sich alle Phononen größerer Wellenlänge im Kristall ausbreiten. Das Zonenrand-Phonon bewirkt eine periodische Modulation der Solvationsenergie der molekularen Ladungstransferzustände, die als Endzustände im Anrege-Abfrage Experiment benutzt werden. Dadurch wird die Detektionseffizienz des molekularen Wellenpaketes mit der ZBP Frequenz f_{P} moduliert.

Abstract

The molecule Br_2 embedded in solid argon is investigated for the first time on the ultrashort domain via femtosecond pump-probe spectroscopy. Coherent intramolecular vibrational wave packet dynamics and coherent host dynamics are identified in the spectra. The electronic B state potential surface is constructed from the experimental periods using the RKR algorithm, and the energy relaxation is quantified over a large range in this state. During the first molecule-cage collision, up to 50 % vibrational energy loss of the wave packet is observed; however, the intramolecular coherence is preserved in the strong interaction. Furthermore, the coherence can even survive nonadiabatic electronic transitions, as is documented for the case of I_2 in solid Kr.

Interferences in vibrational wave packets of Br_2 molecules are controlled in the presence of a solid Ar environment that provides decoherence. A control scheme based on chirped pulses is worked out with help of a numerical wave packet propagation. By applying a negatively or positively chirped excitation pulse, one can set the clock backward or forward respectively in the wave packet propagation.

Based on this mechanism, we present a general scheme to record vibrational decoherence. Wave packets are spatially focused at T_{opt} by applying negatively chirped pulses. From the focusing contrast, we determine a vibrational dephasing time on the B state of $T_{\text{deph}}^{\text{vib}} = 3$ ps corresponding to about 11 vibrational periods, each of 280 fs. Positively chirped pulses advance the formation of fractional revival structures with respect to $T_{\text{deph}}^{\text{vib}}$. By exciting four vibrational levels with such a pulse in an experiment, we observe a 1/6 revival, indicating the vibrational coherence time $T_{\text{vib}}^4 \approx 1.2$ ps for exactly four levels. The required chirp prolongs the pulse duration by a factor of ten to $\Delta\tau = 300$ fs. Electronic dephasing $T_{\text{deph}}^{\text{el}}$ of the $\text{B} \leftarrow \text{X}$ transition restricts the revival control fidelity to parts of the pulse with $\Delta\tau < T_{\text{deph}}^{\text{el}}$, which allows for the determination of $T_{\text{deph}}^{\text{el}} > 300$ fs.

A long lasting coherent oscillation with a sharp frequency $f_{\text{P}} = 2$ THz is observed in $\text{Br}_2:\text{Ar}$ pump-probe spectra. It matches exactly the Zone Boundary Phonon (ZBP) frequency of the solid Ar host. Furthermore, a frequency component with $f_{\text{P}} = 1.5$ THz is observed in $\text{I}_2:\text{Kr}$ pump-probe spectra, matching the Kr crystal ZBP frequency. The value of f_{P} and its phase with respect to the pump pulse do not depend on the B or A state vibrational dynamics. The phonons originate from a Displacive Excitation of Coherent Phonons (DECP) initiated in the electronic $\text{B} \leftarrow \text{X}$ and $\text{A} \leftarrow \text{X}$ transitions. A model calculation shows that an expansion of the electronic density in going from the electronic ground state X to the B or A state kicks the Ar/Kr atoms in the Br_2/I_2 vicinity. Subsequently, a group of host atoms in the (100) plane is decoupled from the intramolecular dynamics. The ZBPs have a vanishing group velocity v_{g} , and therefore they stay in the vicinity of the chromophore, whereas phonons with longer wavelength propagate away from the molecule. The ZBP modulates the solvation energy of the terminal charge-transfer states used in the probe transition from the A and B state and thus the detection sensitivity of the intramolecular molecular wave packet.

Contents

1	Introduction	1
2	Concepts and methods	5
2.1	Coherence	5
2.1.1	Classical coherence	5
2.1.2	Quantum coherence	7
2.2	Dispersion and revivals in Morse oscillators. Focusing with chirped light pulses	10
2.2.1	Morse potential	10
2.2.2	Focusing of wave packets	11
2.2.3	Fractional revivals	13
2.2.4	Nomenclature for dephasing, decoherence and dispersion	18
2.3	Pump-probe spectroscopy	18
2.3.1	Pump-probe method	20
2.3.2	Vibrational energy relaxation in pump-probe spectra	24
2.3.3	Method to determine the vibrational dephasing in a Morse oscillator . .	25
2.3.4	Manipulation of fractional revival structures and their appearance in pump-probe spectra	25
3	Br₂ and I₂ in rare gas solids	31
3.1	Gas phase properties	31
3.1.1	Physical properties	31
3.1.2	Electronic structure of halogens	32
3.1.3	Selection rules and polarization sensitive spectroscopy	34
3.1.4	Gas phase absorption spectra	36
3.2	Molecules in rare gas solids	37
3.2.1	The cage effect	37
3.2.2	Energy shifts of charge-transfer states	39
3.2.3	Absorption and excitation spectra	39
3.2.4	Literature on Br ₂ in rare gas solids	42
4	Experimental setup	45
4.1	Vacuum system and sample preparation	45
4.2	Absorption spectroscopy setup	48
4.3	Ultrashort laser pulses	49
4.3.1	Gaussian pulses	49
4.3.2	Chirping pulses	52
4.3.3	Nonlinear optics	52
4.3.4	Frequency Resolved Optical Gating (FROG)	54
4.4	Laser System	55

4.4.1	CPA system	55
4.4.2	NOPA setup	56
4.5	Pulse characterization	57
4.6	Pump-probe and emission spectroscopy setup	58
5	Spectroscopic results	61
5.1	Absorption spectra	61
5.2	Emission spectra	61
6	Discussion of spectroscopic results	67
6.1	Discussion of absorption spectra	67
6.2	Discussion of emission spectra and assignment of probe windows	73
6.2.1	One-photon probe transitions	73
6.2.2	Two-photon probe transitions	75
7	Ultrafast dynamics	79
7.1	Intramolecular vibrational wave packets of Br ₂ :Ar	79
7.1.1	Pump-probe spectra of the electronic A and B state	79
7.1.2	Polarization sensitive pump-probe spectroscopy	86
7.1.3	A and B state dynamics decomposition	88
7.1.4	Wave packet focusing	90
7.2	Coherent host dynamics	94
7.2.1	Br ₂ in solid argon	94
7.2.2	I ₂ in solid krypton	97
8	Discussion of ultrafast dynamics	103
8.1	Intramolecular dynamics	103
8.1.1	Vibrational periods in the B state	103
8.1.2	Potential construction	106
8.1.3	Vibrational energy relaxation	112
8.1.4	Trajectory for the first excursion of a wave packet	117
8.2	Methods to determine coherences	121
8.2.1	Wave packet focusing and vibrational coherence	121
8.2.2	Control of fractional revivals and electronic coherence	124
8.2.3	Electronic dephasing	129
8.2.4	Comparison to other methods	130
8.2.5	Comparison to other dephasing constants	131
8.3	Coherent phonon dynamics	133
8.3.1	Excitation scheme for coherent ZBP	134
8.3.2	Detection scheme for coherent ZBP	140
8.3.3	Comparison to alternative models	144
9	Summary	147
	Bibliography	151
	Appendix	169

List of Figures

2.1	Schemes of dephasing and dissipation	6
2.2	Vibrational and electronic dephasing	9
2.3	Dispersion and focusing of a wave packet	12
2.4	Model for quarter and half revivals	14
2.5	Wigner function of a wave packet in a Morse oscillator	16
2.6	Wigner functions of fractional revivals.	17
2.7	Revivals in R-t representation	19
2.8	Pump-probe scheme	20
2.9	Franck-Condon picture for the probe transition	23
2.10	Pump-probe spectrum for energy relaxation	24
2.11	Focusing method to determine vibrational dephasing	26
2.12	Control of fractional revival structures	27
2.13	Pump-probe spectra different R_{win} and E_{win}	28
2.14	Probe window width	29
3.1	Vibrational levels in the B state for Br ₂ isotopes	32
3.2	Molecular orbitals of the electronic ground state of dihalogens.	33
3.3	Potential energy surfaces of free Br ₂	33
3.4	Polarization sensitive pump-probe spectroscopy	35
3.5	Gas phase absorption spectrum of Br ₂	36
3.6	Geometry of the chromophore cage	38
3.7	Configuration coordinate picture (Huan-Rhys)	39
3.8	Excitation spectrum of Br ₂ :Ar	41
4.1	Vacuum system	46
4.2	Absorption spectroscopy setup	48
4.3	Spectra of the high pressure Xe lamp	49
4.4	E Field and instantaneous frequency of a chirped pulse	50
4.5	FROG traces of an unchirped and a positively chirped pulse	55
4.6	NOPA setup	56
4.7	Laser, XFROG and pump-probe setup	57
5.1	Transmission and absorption spectrum of Br ₂ :Ar	62
5.2	Fluorescence decay of the charge-transfer states	62
5.3	Ultraviolet fluorescence bands of Br ₂ :Ar	63
5.4	Temperature dependence of the ultraviolet emission bands of Br ₂ :Ar	64
5.5	Pump-probe signals for the different ultraviolet emission bands	65
6.1	Comparison of different Br ₂ absorption spectra	68
6.2	Construction of an absorption spectrum for the bromine C ← X transition.	68

6.3	Comparison of the experimental absorbance with the projection method	69
6.4	Comparison of projection method to Franck-Condon factors	70
6.5	Spectral shift for typical laser pulses after propagating the crystal	72
6.6	Some covalent and charge-transfer states of the Br ₂ molecule	75
6.7	Difference potentials to charge-transfer states for one-photon transitions	76
6.8	Probe pulse energy dependence of the UV fluorescence at 300 and 322 nm.	76
6.9	Difference potentials to charge-transfer states for two-photon probe transitions.	77
7.1	Long time range pump-probe spectra of Br ₂ :Ar probed from 289 to 320 nm	80
7.2	Pump-probe spectra with $\lambda_{\text{probe}} = 339$ nm and variable λ_{pump}	81
7.3	Short time range pump-probe spectra of the Br ₂ :Ar B state	82
7.4	Short time range pump-probe spectra of the Br ₂ :Ar B state	83
7.5	Br ₂ :Ar pump-probe spectra with $\lambda_{\text{pump}} = 530$ nm and variable λ_{probe}	84
7.6	Pump-probe spectra of Br ₂ :Ar with $\lambda_{\text{probe}} = 620$ nm in a two-photon probe process	85
7.7	Polarization dependent pump-probe spectra for Br ₂ :Ar	86
7.8	Polarization dependent pump-probe spectra for I ₂ :Kr	87
7.9	Pump-probe spectra with $\lambda_{\text{pump}} = 600$ nm, $\lambda_{\text{probe}} = 570$ nm	88
7.10	Polarization dependent pump-probe spectra for $\lambda_{\text{probe}} = 620$ nm	89
7.11	Pump-probe spectra with $\lambda_{\text{pump}} = 580$ nm and $\lambda_{\text{probe}} = 600$ nm	90
7.12	Pump-probe spectra of Br ₂ :Ar and reconstructed A,B state dynamics	91
7.13	SFG FROG and FODM of negatively chirped pulse	92
7.14	Pump-probe spectra excited with different chirped pulses	93
7.15	Pump-probe spectra for different excitation chirps	95
7.16	Pump-probe spectrum of Br ₂ :Ar with $\lambda_{\text{pump}} = 520$ nm and $\lambda_{\text{probe}} = 348$ nm	96
7.17	Pump-probe spectra of Br ₂ :Ar with $\lambda_{\text{probe}} = 348$ nm and λ_{pump} varied from 500 to 530 nm.	96
7.18	Normalized pump-probe spectra of Br ₂ :Ar probing the B or the A state	97
7.19	Fourier spectrum of the $\lambda_{\text{pump}} = 520$ nm, $\lambda_{\text{probe}} = 348$ nm transient of Br ₂ :Ar	98
7.20	Pump-probe spectra of I ₂ :Kr under different excitation conditions	98
7.21	Pump-probe spectra of I ₂ :Kr with $\lambda_{\text{pump}} = 520$ nm and λ_{probe} varied	99
7.22	Pump-probe spectra of I ₂ :Kr for fixed $\lambda_{\text{probe}} = 520$ nm and λ_{pump} varied	100
7.23	Fourier spectrum of an I ₂ :Kr pump-probe spectrum	101
8.1	Br ₂ :Ar pump-probe spectra for $\lambda_{\text{pump}} = 570$ nm and variable λ_{probe}	104
8.2	Illustration of the window effect	105
8.3	Squared vibrational frequencies in the Br ₂ :Ar B state	107
8.4	Pump-probe spectrum and scheme of Br ₂ :Ar excited at 510 nm	109
8.5	RKR potential of Br ₂ :Ar	110
8.6	Free Br ₂ molecule included Br-Ar interaction	111
8.7	Br ₂ :Ar pump-probe spectra with $\lambda_{\text{probe}} = 345$ nm pulses and λ_{pump} varied	113
8.8	Apparent periods T of Br ₂ :Ar as a function of the period number	114
8.9	Vibrational energy relaxation rates for Br ₂ :Ar B state	115
8.10	Energy relaxation for different dihalogens in rare gas solids	116
8.11	Trajectory for a wave packet with $\lambda_{\text{pump}} = 530$ nm in Br ₂ :Ar	117
8.12	Ultrafast nonadiabatic transition in I ₂ :Kr	119
8.13	Focusing times T_{opt} as a function of chirp	121
8.14	Comparison of experimental pump-probe spectra to simulations	122
8.15	Simulated Wigner plots and of Br ₂ with negative chirp excitations	123
8.16	Pump pulse spectral shape and pump-probe spectrum with revivals	125

8.17	Simulated revival pattern of Br ₂ in a pump-probe spectrum for different chirps .	126
8.18	Spectra of a 1/6 revival excited by a positively chirped pump pulse	127
8.19	Spatial interference patterns of a advanced 1/6 revival	128
8.20	Population of vibrational levels by a positively chirped pulse	129
8.21	Phonon dispersion relations of solid argon and krypton and coherent host peaks	134
8.22	Cage geometry of I ₂ :Kr. Interaction of I ₂ with Kr and Br ₂ with Ar	138
8.23	Variation of phonon contribution upon changing λ_{probe}	141
8.24	Phonon detection mechanism	142

List of Tables

3.1	Physical constants of I ₂ and Br ₂	31
3.2	Spectroscopic data for the free Br ₂ molecule.	34
3.3	Emission bands of Br ₂ :Ar	42
5.1	Ultraviolet emission bands (1-3) of Br ₂ :Ar	63
6.1	Population of the vibrational levels 1 and 2 for the Br ₂ X state at 20 and 300 K .	67
6.2	Spectroscopic data for Br ₂ :Ar and gas phase	71
6.3	Calculated UV emission bands of Br ₂ :Ar	74
8.1	B state periods T as a function of energy	106
8.2	Morse fits for Br ₂ :Ar vibrational frequencies.	107
8.3	$R_{\text{win}}(\lambda_{\text{probe}})$ for different λ_{probe}	118
8.4	Time constants used in this thesis	130
8.5	Morse parameters for I-Kr and Br-Ar	136

Abbreviations

CARS - Coherent anti-Stokes Raman scattering
 CT - Charge-Transfer
 DECP - Displacive Excitation of Phonons
 DIM - Diatomics In Molecules
 FC - Franck-Condon
 fcc - face centered cubic
 FODM - First Order Delay Marginal
 FROG - Frequency Resolved Optical Gating
 fs - femtosecond ($10^{-15}s$)
 FWHM - Full Width at Half Maximum
 LIF - Laser Induced Fluorescence
 nm - nanometer ($10^{-9}m$)
 NOPA - Noncollinear Optical Parametric Amplifier
 OMA - Optical Multichannel Analyzer
 ps - picosecond ($10^{-12}s$)
 RGS - Rare Gas Solids
 RKR - Rydberg-Klein-Rees
 SFG - Sum Frequency Generation
 SHG - Second Harmonic Generation
 ZBP - Zone Boundary Phonon

Chapter 1

Introduction

The typical time for chemical bond cleavage and reformation is situated in the range of a few femtoseconds to some picoseconds, dictated by the motion of molecular fragments on their potential energy surfaces. Besides analysis of chemical reactions using ultrashort laser pulse spectroscopy [1–3], the possibility to control the reaction arose [4]. In most of these schemes, a *coherence* in the reacting system is a precondition in achieving the goal, and therefore the term "coherent control" has been applied.

By *coherence*, a well defined phase relation among quantum mechanical wave functions is meant. For molecular systems, the wave functions are divided into electronic, vibrational and rotational parts. The coherent superposition of corresponding eigenstates is called an electronic, vibrational or rotational *wave packet* [5].

Coherently coupled eigenstates can show interference patterns. In the optical double slit experiment, the interference pattern can only be observed if the relative phase of the field emerging from the two slits is stable. In an analogous way, one can construct an interference pattern of two quantum states with fixed relative phases. The optical analogy for the interference of more than two eigenstates is a multiple slit or grating experiment. Due to these formal similarities, the field of coherent quantum phenomena is often called "quantum optics" [6]. Coherent control schemes exploit the interference patterns of wave functions to control the output of a reaction. For example, the "Tannor-Rice" method [7,8] uses the interference of intramolecular vibrational wave functions to achieve a control goal.

The decay of coherence is called *decoherence* or *dephasing*.¹ It is induced by the coupling of the coherent system to an environment which provides statistical fluctuations on the phases of eigenstates. This leads to attenuated interferences among the eigenstates.

Dephasing, used here synonymously with decoherence, destroys the premise of coherent control. For an application, the dephasing times of the molecule involved have to be taken into account. In case of free molecules in the vacuum, the electronic, vibrational, and rotational dephasing times are much longer than the timescales of chemical reactions. Molecules solvated in a liquid or solid environment show considerably shorter dephasing times in the range of femto- to picoseconds. The trend in coherent control of chemical reactions moves in the direction of multidimensional systems in solution, often with biological relevance. Besides dephasing and dissipation of energy, the *dispersion* of wave packets is a crucial process. Wave packets on *anharmonic* potentials (which all relevant molecular potentials are) undergo a broadening, however without a loss of phase memory.

This study aims at establishing a basic model for multidimensional systems like organic dyes or biomolecules in solution, and to isolate dissipation, dephasing and dispersion processes. The insight gained in the model can clarify the preconditions for the observation of coherences in complex systems.

¹The terminology will be specified in section 2.2.4.

Rare Gas Solids (RGS) present conceptually simple hosts. They have a large ionization energy which allows for using high intensity laser pulses. The rare gas atoms are spherical because of their closed electronic shells and they form face centered cubic (fcc) crystals at low temperature [9]. The phonon dispersion relations and optical properties of the crystals are well studied [10–12]. The rare gas atoms are chemically inert, thus one can use adapted gas phase potentials for the molecular dopants.

The molecule in RGS system, studied in this thesis, is chosen under the constraint of an ultrafast dissipation and dephasing, since this is generally the case for large molecules in solutions. In RGS, excited electronic states of halogens undergo such fast processes because their vibrational level spacing is close to the Debye frequency. A variety of halogens has been studied before in RGS.

The molecule can be described as a one dimensional vibronic quantum system, if its rotation is blocked in the RGS. The ClF molecule is sitting on a single-substitutional site in RGS [13–19] and undergoes ultrafast angular randomization after excitation [20] and is therefore not appropriate. First experiments on Cl₂, sitting on a double-substitutional site in RGS, indicate it to be a suitable system under the above mentioned constraints. However, the anharmonicity and resulting dispersion on the electronic B state of Cl₂ are so large that only a few vibrational periods of the wave packet can be observed in experiments. The anharmonicity of I₂ molecules is much lower. The electronic B state of I₂ in RGS shows rich vibrational wave packet structure. An enormous amount of pump-probe spectroscopy has been done by Apkarian and coworkers [21–24] and the Schwentner group [20, 25–28]. The Coherent Raman Antistokes Scattering (CARS) however indicates a limited electronic coherence $T_{\text{deph}}^{\text{el}}$ time of less than 100 fs in the B ← X transition [29–34]. Some of the control methods conducted here will need an electronic coherence time of several hundred femtoseconds and therefore, the B state of the I₂:RGS system cannot be used. However, coherent phonon dynamics and an example of coherent spin-flip will be presented for the I₂:Kr system. The electronic ground state X of I₂ in RGS is not of interest for this study, since the CARS spectra indicate a vibrational dephasing time of several hundred picoseconds, much too long in comparison to complex systems.

Combining the preconditions, we conclude that Br₂ in solid Ar should fulfill all requirements. Excitation spectra of the B ← X transition indicate an electronic dephasing of some hundred femtoseconds. The anharmonicity of the B state is in a convenient range that allows for the observation of a few vibrational wave packet periods without major broadening due to dispersion. From the experiments we found that the vibrational dephasing in the electronic B state is in the picosecond domain. Throughout the thesis, the methods and concepts are primarily conducted on the system Br₂ in solid argon.

The ultrafast dynamics of Br₂ has only been studied in two experiments for the free molecule case [35, 36]. Results on ultrafast dynamics of Br₂ in condensed media have not been documented; this thesis presents the first ones. The potential energy surfaces of free Br₂ are documented in literature [37–52]. The electronic potential surfaces can be approximated by Morse potentials very well [53]. The covalent states of Br₂:RGS were studied in absorption and emission spectroscopy [54–66]. The spectra of the charge-transfer states, needed to establish a pump-probe scheme, have been measured by us and are presented in chapters 5 and 6.

To detect the ultrafast vibrational dynamics of the molecule in its environment, the femtosecond pump-probe spectroscopy is applied. By use of a first femtosecond laser pulse (pump), a coherent superposition of vibrational eigenstates (vibrational wave packet) in an excited electronic state (described by a Morse potential) is created. The interference of the vibrational wave functions is interrogated with a second time delayed fs laser pulse (probe).

The wave packet disperses on the Morse oscillator potential of Br₂, since it spans over a

finite range in energy, all of which give rise to different oscillation periods. However, due to the discrete structure of the vibrational levels, the wave packet will revive after some time T_{rev} (determined by the anharmonicity) and regain its narrow shape. The phenomenon is known under the term revival [67–75]. If the vibrational dephasing time $T_{\text{deph}}^{\text{vib}}$ of the molecule in the RGS is larger than the revival time, the decay of coherence among the vibrational eigenstates can be deduced from the pump-probe spectra directly as a decay of revival features [76–78]. If the vibrational dephasing time is shorter than the revival time but larger than the oscillation period T , a new scheme, which is presented in this thesis and a supplementary article [79] has to be applied. The dispersion reduces the modulation contrast on the same timescale as dephasing does. However, dispersion can be suppressed at a distinct time T_{opt} in the evolution by excitation with a negatively chirped pulse (see section 2.2.2). The method has been used before to demonstrate the possibility of vibrational wave packet focusing [80–83]. The scheme will be systematically applied in this thesis to suppress dispersion at a given time T_{opt} and deduce the vibrational dephasing from a background at T_{opt} in the experimental pump-probe spectra (see sections 2.3.3 and 8.2.1).

Apart from full revivals of the vibrational wave packets in Morse oscillators, fractional revivals arise that cause multiples of the fundamental oscillation frequency in the pump-probe spectrum. Using the fractional revivals, information about coherence of a distinct group of vibrational levels can be deduced. Here, the measured vibrational dephasing time $T_{\text{deph}}^{\text{vib}}$ is too short to observe fractional revivals directly. Therefore, a novel scheme to control the fractional revivals of a vibrational wave packet based on chirped excitation pulses is worked out (see section 2.3.4). The revival features are shifted towards the time-zero by a positively chirped excitation pulse. A 1/6 revival, exhibiting the threefold vibrational period, is observed on the B state of Br_2 in solid Ar. From this experiment, a coherence time of four vibrational levels is estimated in section 8.2.2.

The positively chirped excitation pulses used to advance the revival structures in time are actually longer than one oscillation period of the molecule in its excited electronic state. The vibrational wave packet portions created by the first part of the pulse will interfere with the later created parts of the wave packet. Therefore, the electronic coherence between ground and excited state is involved in the coherent preparation of the wave packet (see section 8.2.3). From the pulse duration an electronic coherence time for the $\text{B} \leftarrow \text{X}$ transition of Br_2 in solid Ar is estimated.

The coherent vibrational dynamics is used to deduce a detailed picture of the molecule-host interaction. We are able to construct an effective intramolecular B state potential for Br_2 in solid Ar in section 8.1.2. Furthermore, the vibrational energy relaxation of wave packets on the electronic B state is determined (section 8.1.3) and a representative trajectory of a vibrational wave packet is shown (section 8.1.4). For the case of $\text{I}_2:\text{Kr}$, the vibrational coherence even survives vibrational energy losses of 1 eV connected to a spin-flip transition to another electronic state (section 8.1.4).

It will turn out that the interaction of the vibrating molecule with the matrix is not necessarily statistical. In contrast, collisions of the molecule with the matrix can lead to the creation of coherent wave packets built from vibrational levels not populated before the collision.

Coherent motions are found even for host atoms, showing up in the pump-probe spectra of the molecular guest. The conflictive issues of the specific mode, together with its excitation and probe mechanism were discussed in [24,29,30,32,84–86]. We attribute the coherent host motion to a Zone Boundary Phonon (ZBP) of the rare gas crystal. To support assignment, spectra of $\text{I}_2:\text{Kr}$ (also measured by the author) are presented alongside the spectra of $\text{Br}_2:\text{Ar}$, both showing the coherent ZBP signature. The excitation of the coherent host phonon is achieved via the

expansion of the molecular electronic cloud during the $A \leftarrow X$ or $B \leftarrow X$ transition. This scheme is very similar to the model of Displacive Excitation of Coherent Phonons (DECP) [87–95] and will be presented in section 8.3.1. Many different phonon modes are excited, but only the ZBP having a vanishing group velocity stay at the excited molecule. They change the local density in the vicinity of the chromophore and thereby change the solvation energy of the molecular charge-transfer states [86, 96, 97], which in turn modulates the probe transition efficiency (see section 8.3.2).

Several theory groups treat the halogen in RGS systems extensively and their efforts have, to a large extent, motivated our experiments. Classical and quantum mechanical simulations mostly based on the DIM (Diatomics In Molecules) [98–103] approach give a detailed picture of the dynamical processes of molecular guests in a RGS host. Besides calculations on small molecules F_2 , HCl , and Cl_2 in rare gases [104–108], simulations of the heavier I_2 molecules in rare gas environments exist [109–116]. Up to now, no simulations of the Br_2 in RGS have been published. Due to the results presented in this thesis, a collaborative effort within the Sfb 450² with the groups of Prof. Manz and Prof. Gerber aims to perform such calculations.

This thesis is organized as follows:

Chapter 2 introduces the basic ideas of coherence, dephasing, dispersion and fractional revivals. Furthermore, the ultrafast pump-probe spectroscopy and the methods used to determine vibrational and electronic dephasing times are explained.

The potential energy surfaces of the free Br_2 molecule and the general effects of the RGS on the spectroscopic molecular properties are presented in chapter 3. The experimental setup is described in chapter 4, together with a summary of ultrashort (chirped) laser pulses. The chapters 5, 6 on absorption and emission spectroscopy provide the information needed to conduct fs pump-probe spectroscopy on the system $Br_2:Ar$.

Chapter 7 presents the first results on $Br_2:Ar$ dynamics, where one- and two-photon probe processes are used to detect vibrational wave packet dynamics. The rotation of the molecule is proved to be frozen. Furthermore, the coherent host motion in $Br_2:Ar$ and $I_2:Kr$ is illustrated.

The vibrational wave packet dynamics is used to determine an effective molecule-matrix potential for the electronic B state of Br_2 in solid Ar in chapter 8.1. Furthermore, the vibrational energy relaxation and an experimental trajectory are calculated in this section. The results on vibrational and electronic dephasing in $Br_2:Ar$ are discussed in chapter 8.2. This chapter ends with the discussion of the coherent zone boundary phonon in $I_2:Kr$ and $Br_2:Ar$ (chapter 8.3).

²The collaborative research center SFB 450 is also financing and supporting this experimental work.

Chapter 2

Concepts and methods

Part 2.1 of this chapter will introduce the concepts of coherence, which is a central issue in this thesis. This will be followed by a presentation of dispersion, wave packet focusing and fractional revivals in section 2.2. The pump-probe method and the wave packet control schemes are presented in the final section 2.3 of this chapter.

2.1 Coherence

This section will provide the definition of coherence needed throughout the thesis. It is necessary to have the ideas of coherence in mind to follow the sections to come.

It is reasonable to start from the classical idea of coherence, defined for an ensemble of trajectories in phase space. For convenience, the dephasing and dissipation processes will be explained using a harmonic oscillator potential. The step from classical coherence to quantum coherence is made with the help of the density operator. Since the harmonic approximation is not sufficiently accurate for diatomic molecular electronic potentials, the Morse potential and the propagation of classical trajectories and quantum mechanical wave packets on it will be discussed afterwards. This will lead to the definition of dispersion and fractional revivals of a vibrational wave packet.

2.1.1 Classical coherence

The electronic state of a diatomic molecule is presented in the harmonic approximation. The molecules are elongated from the equilibrium distance (for example in an optical transition) and an oscillatory motion of the molecular ensemble sets in. The classical molecular ensemble shall have a finite width in the spatial distribution, inducing also a finite width in the momentum distribution. The ensemble is represented in phase space. One dimension describes the elongation q of the oscillators, the other dimension the momentum p . The distribution of oscillators is represented as a grey shaded area in phase space as shown in Fig. 2.1.

The molecules are considered as oscillating freely in Fig. 2.1a. The q and p axis of phase space shall be scaled such that q^2 represents the potential energy and p^2 the kinetic energy. For that case the total energy is given by $r^2 = q^2 + p^2$, where r is the distance to phase space origin. Since the energy of each oscillator is conserved, the value of r is not changed in the propagation. Apart from this, the angle α which the ensemble spans from the phase space origin is also not changed in the course of time. The propagation is said to be completely coherent in the case described in Fig. 2.1a.

Next, statistical elastic collisions with an environment are introduced. The molecular oscillators will not lose any vibrational energy in the collision, but the phase of an individual oscillator is changed by a small random value. The molecular oscillator will jump to another position in phase space, nevertheless keeping the same energy (*i.e.* r^2). The change of the molecular ensemble in this *dephasing* process is shown in Fig. 2.1b. The angle α gets broader in the

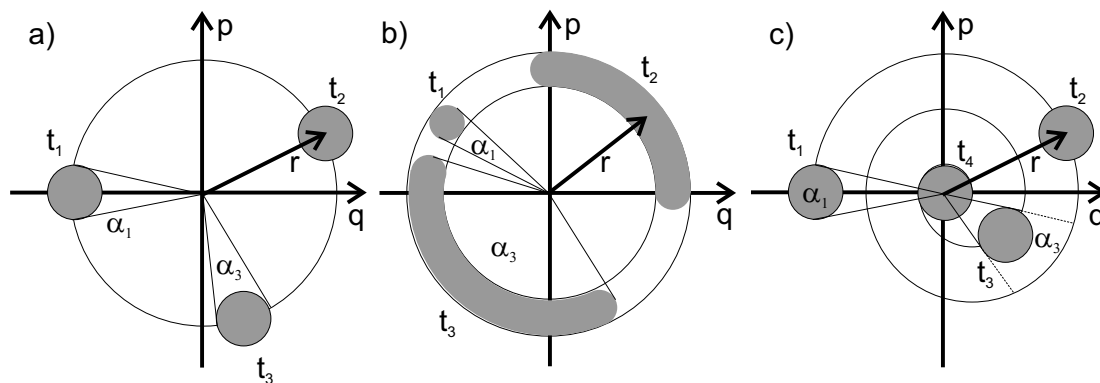


Figure 2.1: a) An ensemble of free classical harmonic oscillators in phase space position (q, p) (position, momentum) is shown as the grey area. No dephasing or dissipation occurs and the angle α under which the ensemble is seen from the origin of phase space does not change in the course of time ($t_1 < t_2 < t_3$). The radius r being proportional to the average energy is also constant in time. b) Case of pure dephasing. The molecules suffer statistical elastic collisions with an environment. The phase of a single molecular oscillator is changed by a small random value in a collision. The angle α for the ensemble average grows with propagation time ($\alpha_1 < \alpha_3$). c) Dissipative case. The molecules suffer inelastic collisions with a bath. The absolute width of the ensemble shall not be changed (no pure dephasing). The mean energy decreases as a function of time and the ensemble spirals to the potential minimum in the origin of the phase space plot. Furthermore, α increases with time, indicating the connection of dissipation and dephasing (form Ref. [73]).

course of time, with $\alpha_3 > \alpha_1$ for ($t_3 > t_1$). With increasing time, the molecular oscillator ensemble will fill the complete iso energetic ring depicted in Fig. 2.1b with a corresponding angle $\alpha = 2\pi$. Such an ensemble would be called completely incoherent or completely "*dephased*". Each molecule would still fulfill a harmonic oscillation, but its phase cannot be predicted, since the elastic collisions occur statistically. The same effect would occur, if the oscillation frequency would be slightly different for the groups of molecules. For example, some molecules can be heavier than others, as is the case for different molecular isotopes. Such a broadening of the angle α due to a splitting of the ensemble in groups with different oscillatory properties will be called in general *inhomogeneous*, while broadening effects being the same for every member will be generally called *homogenous*.

Apart from elastic collisions, inelastic collisions also occur in the investigation. The effect is called *dissipation*, or in the special case described in this thesis vibrational energy relaxation, and is illustrated in Fig. 2.1c. The molecular ensemble loses energy and spirals towards the center of phase space. The molecular ensemble propagates to smaller distances in r but keeps the width in q and p , since the phase of an individual oscillator is not changed. Connected with the loss of energy is the broadening of the angle α . Therefore, dephasing is directly connected to dissipation and cannot be avoided. When the vibrational ensemble has relaxed to the center of phase space, α is equal to 2π . To distinguish the dephasing induced by dissipation (Fig. 2.1c) from the dephasing described in Fig. 2.1b, the latter is often called *pure dephasing*.

The classical coherence introduced above can indeed be used to describe many experiments. Apkarian and coworkers, for example, have used classical trajectories for a calculation of pump-probe experiments [22–24]. However, the interference phenomena cannot be simulated in the classical approach. The quantum coherence is therefore introduced in the next section. The picture developed for a completely classical ensemble of molecules deserves to introduce the

term of quantum coherence here.

2.1.2 Quantum coherence

The n th eigenfunction $|\phi_n\rangle$ in a potential shall belong to energy eigenvalue E_n . A wave packet $|\Psi(t)\rangle$ can be written as a superposition of energy eigenfunctions :

$$|\Psi(t)\rangle = \sum_n c_n e^{-i\frac{E_n t}{\hbar}} |\phi_n\rangle, \quad (2.1)$$

where c_n are the excitation coefficients. The $|\phi_n\rangle$ can be vibrational, rotational or electronic eigenfunctions of the molecule.

In order to define the quantum coherence properly, one has to consider the density operator ρ :

$$\rho = \sum_i p_i |\Psi_i\rangle \langle \Psi_i|. \quad (2.2)$$

$|\Psi_i\rangle$ is a wave function or wave packet. The p_i are the statistical probabilities of finding the system in the state $|\Psi_i\rangle$. They have to fulfill the condition:

$$\sum_i p_i = 1.$$

The state is called *pure*, if there is one i for which $p_i = 1$ and all the other $p_j = 0$ ($i \neq j$). In any other case, the state is said to be *mixed*. Let $\rho(x', x)$ be the density operator in the position representation of $|\Psi(t)\rangle$, which is a wave packet according to Eq. (2.1). Then:

$$\begin{aligned} \rho(x', x) &= \langle x' | \Psi(t) \rangle \langle \Psi(t) | x \rangle \\ &= \sum_{m,n} \langle x' | \phi_m \rangle \langle \phi_m | \Psi(t) \rangle \langle \Psi(t) | \phi_n \rangle \langle \phi_n | x \rangle \\ &= \sum_{m,n} \phi_m(x') (c_m e^{-i\frac{E_m t}{\hbar}}) (c_n^* e^{+i\frac{E_n t}{\hbar}}) \phi_n^*(x) \\ &= \sum_{m,n} \phi_m(x') \rho_{mn} \phi_n^*(x), \end{aligned} \quad (2.3)$$

with $\rho_{mn} = c_m c_n^* e^{-i\frac{(E_m - E_n)t}{\hbar}}$ being the density operator (matrix) in the energy representation. A simple example to illustrate ρ_{mn} shall be given in a two-state system:

$$\rho_{mn} = \begin{pmatrix} |c_1|^2 & c_1 c_2^* e^{-i\frac{(E_1 - E_2)t}{\hbar}} \\ c_1^* c_2 e^{-i\frac{(E_2 - E_1)t}{\hbar}} & |c_2|^2 \end{pmatrix} \quad (2.4)$$

The diagonal elements of the density matrix are called populations. The off-diagonal elements are called quantum *coherences*. In contrast to the diagonal elements, they are complex and oscillate in time with a frequency corresponding to the energy difference.

These coherences are crucial for the development of interference patterns between the different eigenfunctions, as shall be explained for a system consisting of two vibrational eigenfunctions $\phi_0(R)$ and $\phi_1(R)$ with energies $E_0 = \frac{1}{2}\omega_e$ and $E_1 = \frac{3}{2}\omega_e$. The wave packet is written as: $\Psi(R, t) = c_0 e^{-i\omega_e(0+\frac{1}{2})t} \phi_0(R) + c_1 e^{-i\omega_e(1+\frac{1}{2})t} \phi_1(R)$. One obtains the probability density: $|\Psi(R, t)|^2 = |c_0|^2 |\phi_0(R)|^2 + |c_1|^2 |\phi_1(R)|^2 + 2\text{Re}(c_0^* c_1 \phi_0^*(R) \phi_1(R) e^{-i/(E_1 - E_0)t/\hbar})$. The interference term in the last equation is based on the real part of the coherence of the density

operator. If this coherence vanishes, only the incoherent superposition given by the first two terms (populations) in the last equation remain and any time-dependent behavior of the wave packet is cancelled.

If the entity

$$\text{Tr}(\rho\rho) = 1. \quad (2.5)$$

is fulfilled, the system is called *coherent*. A pure state is coherent *per se*. A mixed state of n pure states will be called *partially coherent*, if $1 > \text{Tr}(\rho\rho) > 1/n$. A state is called *incoherent* if $\text{Tr}(\rho\rho) = 1/n$.

The question of how to describe the dephasing and dissipation processes in quantum mechanics arises. The Liouville-von Neuman equation gives the propagation of ρ by:

$$i\hbar \frac{\partial \rho}{\partial t} = [H, \rho] + \Gamma \rho, \quad (2.6)$$

where Γ is a tensor describing the dissipation and dephasing. Without Γ , the equation is equal to the Schrödinger equation. Descriptions of Γ were given for example by Redfield [117, 118] or Lindblad [119, 120]. In contrast to these studies, the processes here are treated empirically.

The density operator in phase space is discussed and compared to the classical density shown in Fig. 2.1. This "phase space approach" is taken from D. Tannor [73, 121, 122]. For that reason, the Wigner transformation of the density operator has to be defined. The Wigner function $f_W(q, p)$ is a very natural way to describe the density operator. For a pure state it is given as:

$$f_W(q, p) = \frac{1}{2\pi\hbar} \int_{-\infty}^{\infty} e^{i\frac{p}{\hbar}(x-x')} \langle x' | \rho | x \rangle ds = \frac{1}{2\pi\hbar} \int_{-\infty}^{\infty} e^{i\frac{p}{\hbar}(x-x')} \langle x' | \Psi \rangle \langle \Psi | x \rangle ds, \quad (2.7)$$

where $x = q + s/2$ and $x' = q - s/2$. Thus $f_W(q, p)$ is the Fourier transform of $\langle x' | \Psi \rangle \langle \Psi | x \rangle = \Psi(x')\Psi^*(x)$ along the difference coordinate $s = x - x'$. When interpreting q as a position (for example the internuclear distance R in case of a molecular vibrational wave packet), the corresponding interpretation of p would be momentum. The projections of the Wigner functions on q or p show the absolute square of the wave packet on the respective coordinate. Nevertheless, $f_W(q, p)$ itself might become negative. This is in contradiction to its assignment as an analogue to classical phase space probability distribution, which is discussed in the literature [73].

The phase space representation of a vibrational wave packet on a harmonic potential¹ can be compared to Fig. 2.1. In order to achieve an increasing angle α as in Fig. 2.1b, a rate constant T_2^* has to be introduced and the coherences (off diagonal elements) of the density matrix in energy representation have to be multiplied by a factor $e^{-t/(|n-m|T_2^*)}$, where n describes the row and m the column of the density matrix [73]. The populations (diagonal elements) stay untouched. The nomenclature for the rate constants is adapted from the Bloch equations in NMR spectroscopy [123]. Here they are defined for a multi-state system instead of only a two level system as in NMR.

The populations of the density matrix will decay if *dissipation* (or in the special case of the molecular potential, *vibrational energy relaxation*) occurs. In order to produce the phase space propagation in Fig. 2.1c with the Wigner transformation of a density operator, a time constant T_1 has to be introduced. It acts on the populations by the decay term e^{-t/T_1} and on the coherence by the decay $e^{-t/2T_1}$ [73]. In a mixed case of pure dephasing and dissipation, a new dephasing time T_2 can be defined in a two-level system with the dissipation T_1 and pure dephasing T_2^* :²

$$\frac{1}{T_2} = \frac{1}{2T_1} + \frac{1}{T_2^*}. \quad (2.8)$$

¹The evolution on an anharmonic oscillator will be the topic of the next section.

² T_1 will be used throughout this thesis for dissipation, whereas T_2 will be substituted by T_{deph} .

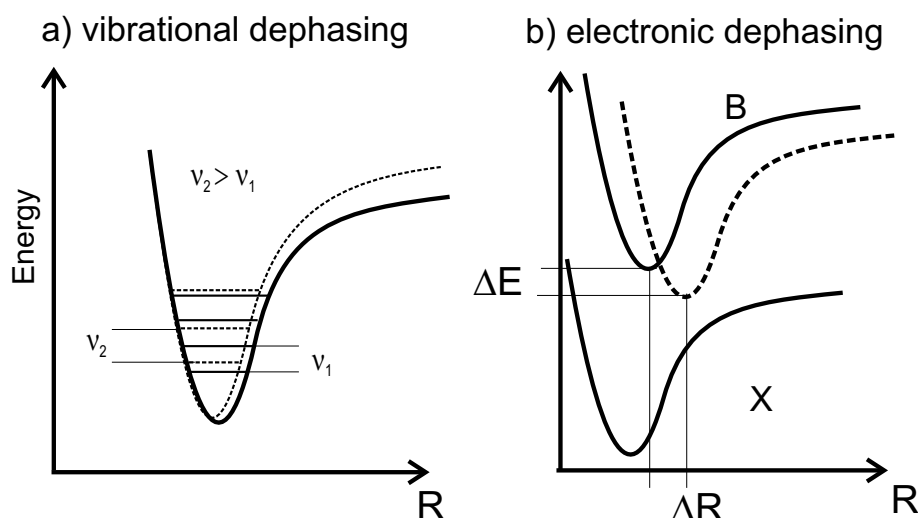


Figure 2.2: a) Scheme for vibrational dephasing. The effective molecular electronic potential $V(R)$ changes due to molecule solvent coordinate changes. The cage is tightening in this example (dashed line). This shifts the vibrational spacing from ν_1 to ν_2 . b) Scheme for electronic dephasing. The transition energy from one electronic state X to another state B is changed by ΔE and/or ΔR .

The Born-Oppenheimer approximation is inherent in the separation of electronic and vibrational degrees of freedom and thus in the separation of dephasing processes. The motion of the electrons is fast compared to the nuclear motion in a molecule and therefore the electronic wave function can be calculated for a fixed set of nuclear parameters. This leads to the calculation of electronic potentials $V(R)$, having defined vibrational and rotational wave functions. The coherences of the density operator have the form $c_n c_m^* e^{-\frac{i}{\hbar}(E_n - E_m)t}$. States n and m can be vibrational levels on one electronic surface $V(R)$ of the molecule. If the coherence term vanishes, the process is called *vibrational* dephasing. In the same manner, state n can be a vibrational state on the electronic ground state, whereas state m is a vibrational level on an excited electronic state of a molecule. In that case, the loss of coherence is called *electronic* dephasing.

Figure 2.2 presents possible origins of vibrational and electronic dephasing. In panel a), the vibrational dephasing is sketched (the picture is adapted from Ref. [78]). The solid curve represents the molecular potential as it is deformed in some solvent. The vibrational eigenstates of the potential shall have an energy spacing of ν_1 . If a relative motion between molecule and solvent atoms occurs, this potential energy surface will be disturbed (dashed line). As sketched here, the effective intramolecular potential gets steeper and the vibrational spacing ν_2 bigger than ν_1 . This leads to a disturbance (dephasing) in the coherence of the vibrational levels n and m , since the energy difference³ $(E_n - E_m)$ between the vibrational levels n and m shows up in the coherence $c_n c_m^* e^{-\frac{i}{\hbar}(E_n - E_m)t}$. Thus, the wave packet will lose coherence and interference of vibrational levels will decay. As a consequence, the probability density loses its localization in phase space according to the classical dephasing in Fig. 2.1b. The effect can also be formulated in semi classical terms: the wave packet propagates in a dynamical potential. The dynamics of the effective potential is statistical in an ensemble. A wave packet of a *single* molecule does not dephase at all. In an *ensemble* or time-averaged experiment the averaged wave packet structure will "smear out". The calculation in Ref. [78] is done in exactly that way: a quantum wave packet is propagated on a dynamical potential that is calculated by classical interaction with the environment. The final result is averaged over many wave packet propagations.

In case of the electronic dephasing (Fig. 2.2b), the relative energy or/and equilibrium poten-

³Between two neighboring levels, the difference is called ν in Fig. 2.2.